ACSNANO

www.acsnano.org

ARTICLE

Aromatic Bridged Bis(triphenylamine) Cascade Assembly Achieved Tunable Nanosupramolecular Morphology and NIR Targeted Cell Imaging

Jie Yu, Jie Niu, Jinlong Yue, Li-Hua Wang, and Yu Liu*

Cite This: https://doi.org/10.1021/acsnano.3c06697

Read Online

ACCESS | Metrics & More | Article Recommendations | Supporting Information

ABSTRACT: Possessing four cationic pyridium groups, phenyl-bridged bis(triphenylamine) derivatives (G1, G2) were encapsulated by cucurbit[8]uril (CB[8]) at a 1:2 stoichiometry to form the network-like organic two-dimensional nanosheet, which could efficiently enhance the near-infrared (NIR) luminescence and companies with a red-shift from 750 to 810 nm for G1. Benefiting from the supramolecular multivalent interaction, α-cyclodextrin modified hyaluronic acid (HACD) and G1/CB[8] formed nanoparticles to further enhance NIR luminescence behaviors. Compared with the short rigid aromatic bridged bis-(triphenylamine) derivative (G2), the supramolecular assembly derived from G1 with long flexible cationic arms gives a larger Stokes shift, which further coassembles with the phosphorescent bromophenylpyridinium derivative/CB[8] pseudorotaxane, leading to efficient phosphorescent resonance energy transfer (PRET). Especially, the nanoparticle showed delayed NIR fluorescence under 308 nm light excitation with an ultralarge Stokes shift up to 502 nm, which was successfully applied in targeted NIR cell imaging.

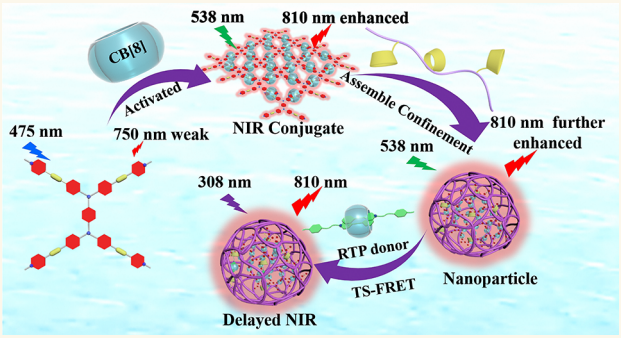

KEYWORDS: *cucurbituril, cyclodextrin, supramolecular assembly, energy transfer, NIR luminescence*

INTRODUCTION

Recently, aggregation-induced emission (AIE),[1] photon-upconversion,[2] aggregation-induced photocatalytic activity,[3−5] and nanosupramolecular cascade assembly based on macrocyclic confinement have become the hot topics in supramolecular chemistry and are widely applied in biological imaging,[6] energy transfer,[7] sensing detection,[8] gel,[9] catalysis,[10] and nanofilms.[11] Especially, the strategy of macrocyclic and assemble confinement can not only realize the noncovalent polymerization of assemble units to form ordered nanostructures but also improve their photophysical properties. In the process of investigating macrocyclic confinement, cucurbit[n]-uril (CB[n]) and cyclodextrin could act as excellent candidates. First, the CB[n] with a hydrophobic cavity was synthesized by the condensation of glycoluril and formaldehyde, which could encapsulate neutral and cationic guests to form supramolecular assemblies.[12,13] For example, Scherman[14] and co-workers reported that CB[8] included the guest molecules with pyridine salts at a 2:2 stoichiometry to form dimeric stacked fluorophores, achieving tunable supramolecular structure and fluorescence properties. George[15] found that cationic bromophthalimide derivatives emit efficient blue phosphorescence under the confinement of CB[7], especially, which could cascade assemble with laponite and dye acceptors, giving multicolor luminescent supramolecular hydrogels. Li et al.[16] reported that pyridine-modified carbazolyl derivatives could assemble with different molar ratios of CB[8] to form one-dimensional nanobelt, two-dimensional nanoplate, and three-dimensional polyhedron, accompanied by the color of the fluorescence change from blue to orange. We constructed a supramolecular assembly of CB[8] confined anthracene-modified bromophenylpyridinium at 1:2 stoichiometry, which when located in the nucleus gave red fluorescence and in

Received: July 20, 2023
Accepted: September 26, 2023

Scheme 1. Aromatic Bridged Bis(triphenylamine) Cascade Assembly Achieved Tunable Nanosupramolecular Morphology and NIR Luminescence

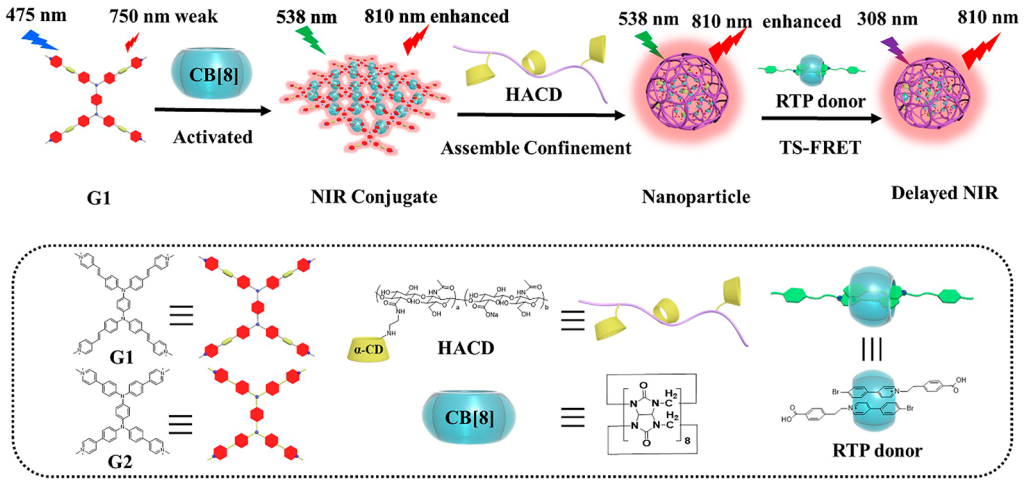

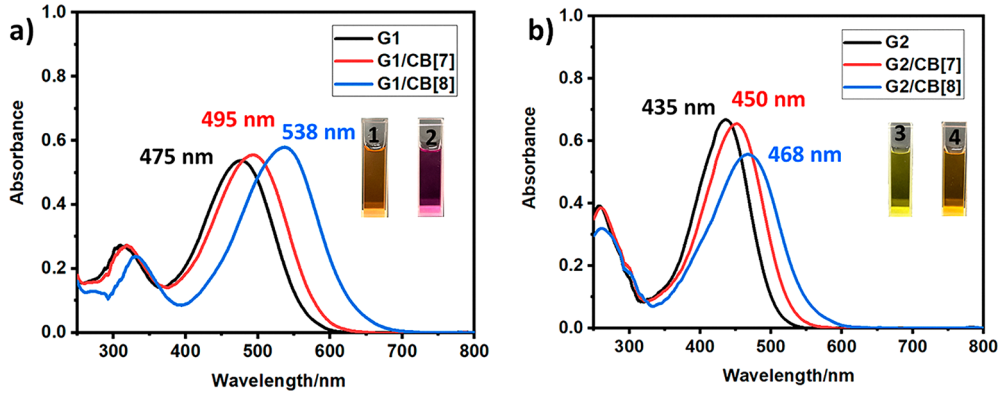

Figure 1. (a) UV−vis spectra of G1, G1/CB[7] and G1/CB[8] in H_2O, Inset: (1) G1, (2) G1/CB[8]. (b) UV−vis spectra of G2, G2/CB[7] and G2/CB[8] in H_2O, Inset: (3) G2, (4) G2/CB[8] ([G1] = [G2] = 0.01 mM, [CB[7]] = 0.04 mM, [CB[8]] = 0.02 mM).

lysosomes gave green phosphorescence, respectively, showing double organelle imaging ability-driven by a photoreaction.[17] As compared with CB[n], cyclodextrin (CDs) possess hydrophobic cavities and hydrophilic surfaces, which could encapsulate anionic or neutral guest molecules.[18,19] For example, Tang et al. reported that β-cyclodextrin induced p-biphenylboronic acid to give second-level lifetime phosphorescence in water.[20] We found that γ-cyclodextrin could encapsulate a triphenylene boronic acid derivative unit grafted noncovalent polymer based on poly(vinyl alcohol) to give an ultralong phosphoresce lifetime up to 5.84 s, and then after being further doped with dyes as acceptors, forms the full-color delayed fluorescence afterglow materials.[21] Therefore, taking different advantage of the CB[n] and CDs binding with anionic, cationic guest molecules to achieve the secondary assembly, not only regulates the topological morphology of the nanosupramolecules but also is conducive to the modulation of luminescence properties. We also reported the configurationally confined cascade nanosupramolecular assembly, which was constructed by CB[8], cationic tetraphenylpyridium derivative, and negatively charged β-cyclodextrin, modulating the topological morphology change from nanoparticles to nanosheets and realized the multicolor fluorescence by the energy transfer process.[22] However, adopting CB[n] and CDs, two kinds of hydrophobic macrocycle cascade confinement, to enhance the PRET and NIR luminescence with a large Stokes shift has not been reported, to the best of our knowledge.

In the present work, we reported that when phenyl-bridged dual triphenylamine derivatives were encapsulated by CB[8] at a 1:2 stoichiometry, the macrocyclic confinement not only efficiently achieves the NIR emission with a 60 nm red-shift but also gives a positive network-like organic two-dimensional nanosheet, which can undergo a secondary assemble with targeted agent HACD to form three-dimensional nanoparticles, boosting the NIR fluorescence emission. Especially, this endows the nanoparticles with the ability to load energy donor or acceptor by the host−guest interaction of α-cyclodextrin, leading to the delayed NIR luminescence and photoregulation red fluorescence emission from an efficient energy transfer process. The NIR supramolecular nanoparticles were successfully applied in targeted lysosome cell imaging, photoregulated logic gate, and information encryption, which provided a convenient method for tunable multidimensional supramolecular assembly with large Stokes shift (Scheme 1).

RESULTS AND DISCUSSION

Two kinds of phenyl-bridged dual triphenylamine derivatives with four flexible (G1) or rigid cationic pyridium groups (G2) were synthesized by the Suzuki−Miyaura coupling reaction and further quaternization of pyridine groups to give water-soluble guests (Scheme S1), which were characterized by

https://doi.org/10.1021/acsnano.3c06697
ACS Nano XXXX, XXX, XXX−XXX

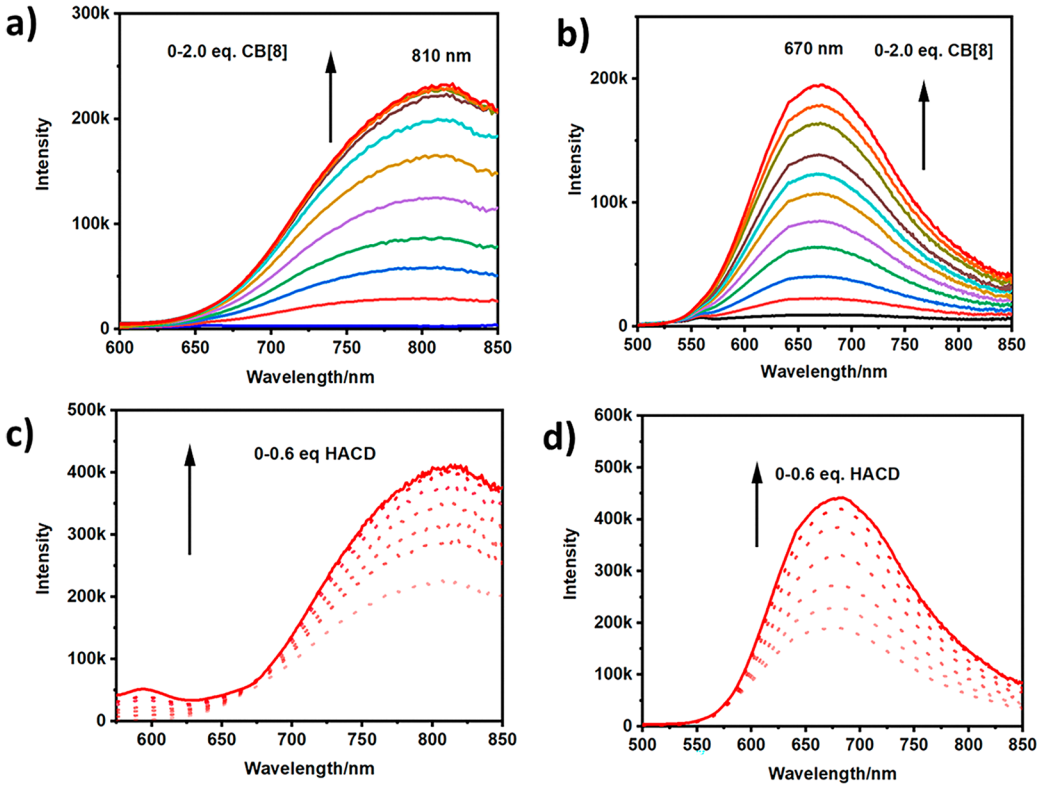

Figure 2. (a) Fluorescence spectra of G1 in the presence of CB[8] (λ_{ex} = 538 nm). (b) Fluorescence spectra of G2 in the presence of CB[8] (λ_{ex} = 468 nm, [G1] = 0.01 mM). (c) Fluorescence spectra of G1/CB[8] in the presence of HACD (λ_{ex} = 538 nm). (d) Fluorescence spectra of G2/CB[8] in the presence of HACD (λ_{ex} = 468 nm, [G1] = [G2] = 0.01 mM, and [CB[8]] = 0.02 mM).

nuclear magnetic resonance (^{1}H NMR, ^{13}C NMR) and high-resolution mass spectrometry (Figures S1–S6). UV–vis spectroscopy experiments were performed to investigate the binding behavior between CB[8] and two guests. The absorption peak of G1 was red-shifted from 475 to 538 nm (Figure 1a), and the solution of G1 was changed from yellow to purple after adding CB[8], which was probably due to the pyridinium groups of G1 being penetrated in CB[8] cavities to give J-aggregates.[23] In sharp contrast with G1/CB[8], the absorption peak of G1 gave a 20 nm red-shift after the addition of CB[7], which may be attributed to the obtained supramolecular complexes being different from G1/CB[8] under the confinement of CB[7]. Possessing short rigid cationic arms, G2 was also encapsulated by CB[8], and the absorption signal was red-shifted from 435 to 468 nm (Figure 1b). The Job plot showed that the inflection point occurred at a molar fraction of 0.33, indicating a 1:2 stoichiometry between G1 (or G2) and CB[8] (Figure S11). In this system, CB[8] could bind two pyridinium units by the "head to tail" mode in G1 or G2, avoiding positive charge repulsion, and then give supramolecular complexes, which is also consistent with the 1:2 stoichiometry obtained from the Job plot. Furthermore, according to the result of UV–vis titration experiments (Figures S12–S13), the binding constants (K_s) between the two guest molecules and CB[8] were measured to be 2.23 × 10^9 M^{-2} and 3.79 × 10^8 M^{-2}, and the equilibrium concentrations of CB[8] were 11.34 μM and 17.68 μM (when the total concentration of CB[8] = 0.02 mM), respectively, indicating two kinds of guests were encapsulated by CB[8] to give stable host–guest complexes. It is noteworthy that the binding constant between CB[8] and G1 is obviously larger than that between CB[8] and G2, which may be attributed to the G1 with the flexible longer conjugated arms then easy to form J-aggregates under the confinement of CB[8].

NMR experiments were also performed to explore the binding model between the guests and CB[8] in solution. In the presence of 0.5 eq. CB[8] (Figure S14), the protons of $H_{c,d}$ gave larger upfield shifts than $H_{a,b,e}$ in G1, indicating the flexible conjugated cationic pyridium groups of G1 were encapsulated by the host.[24−26] With the continuous addition of CB[8], the protons of the G1 were broadened and difficult to identify, which may be ascribed to the formation of more extended supramolecular noncovalent polymers in solution.[27,28] The signals of the protons in G2 were also broadened and upfield shifted, manifesting the formation of the supramolecular conjugate of G2/CB[8] (Figure S15). 2D NOESY data of G1/CB[8] and G2/CB[8] (Figures S16–S17) showed that the protons of the cationic pyridium groups correlated to the protons of CB[8] (3.8–4.2 ppm), which further confirmed that the cationic arms of guests were located in CB[8] cavities and may further assemble to give a large extent conjugates. Furthermore, the 2D DOSY result manifested that the diffusion coefficient values of G1 and G2 decreased from 1.50 × 10^{-10} m^2/s to 1.07 × 10^{-10} m^2/s, and 2.26 × 10^{-10} m^2/s to 1.23 × 10^{-10} m^2/s, respectively (Figures S18–S19), indicating supramolecular complexes assemble to form larger assemblies than the guests. The hydrodynamic sizes of G1/CB[8] and G2/CB[8] were measured to be 1.31 and 1.63 μm, respectively (Figures S20), and these experimental results basically exclude simple dimeric stacked type host–guest complexes.[17]

https://doi.org/10.1021/acsnano.3c06697
ACS Nano XXXX, XXX, XXX–XXX

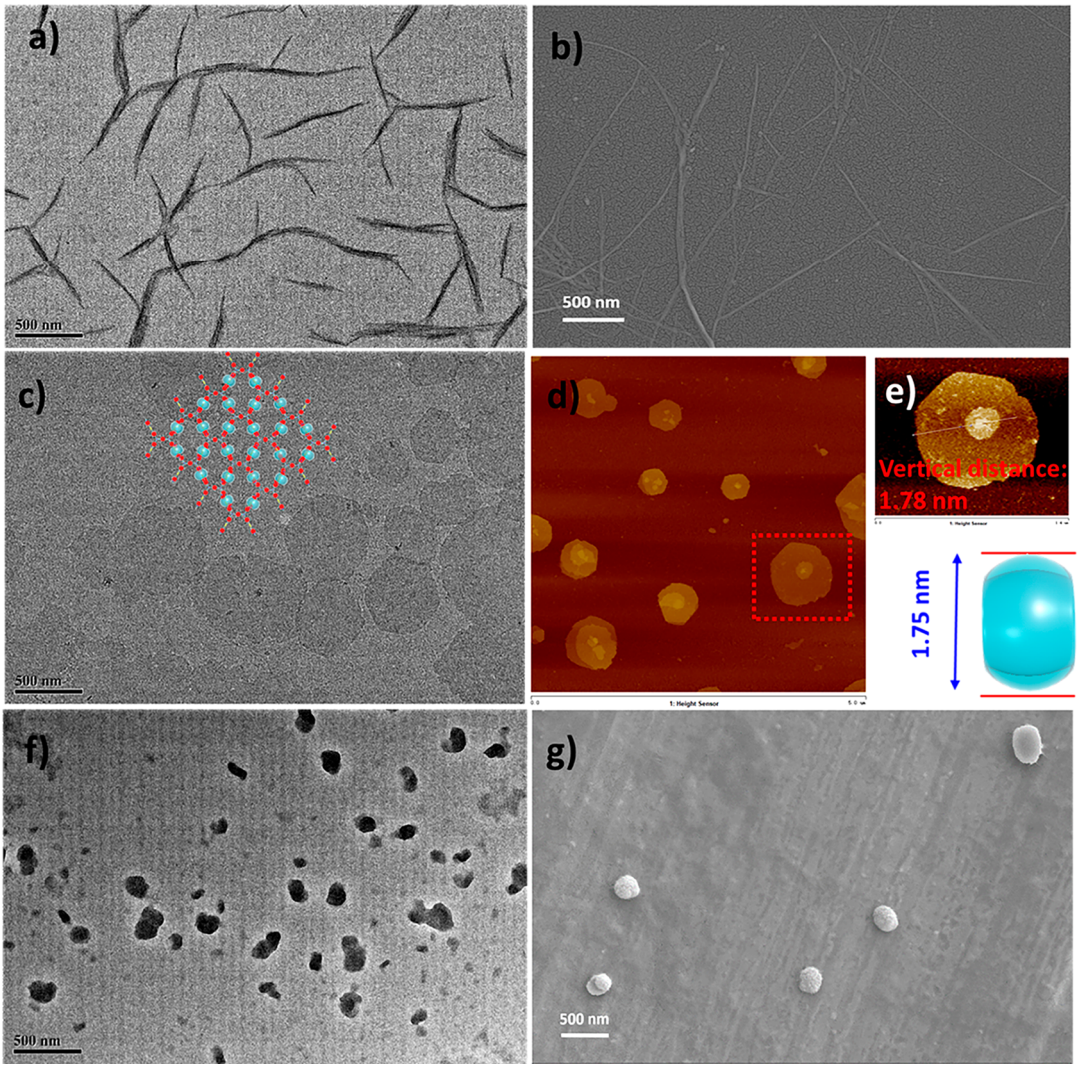

Figure 3. (a) TEM and (b) SEM images of G1. (c) TEM and (d, e) AFM images of G1/CB[8]. (f) TEM and (g) SEM images of G1/CB[8]/HACD.

In order to confirm the influence of the CBs confinement effect on the luminescence properties of aromatic bridged bis(triphenylamine) derivatives, fluorescence titration experiments were performed. As shown in Figure 2a, the guest G1 showed a very weak fluorescence signal at 750 nm; however, a NIR fluorescence peak was generated and gradually increased at 810 nm in the presence of CB[8], leading to a large Stokes shift up to 272 nm. Compared with G1, possessing short rigid arms, G2 also showed enhanced fluorescence at 670 nm but only gave a 25 nm red-shift and a minor Stokes shift (202 nm) under the confinement of CB[8] (Figure 2b), which may ascribed to the G1 with longer flexible structure being beneficial to the deep inclusion of CB[8], and then formed a more extended and conjugated supramolecular polymer. The fluorescence quantum yields (QY) of G1 and G2 were also increased from 0.01% and 0.06% to 0.10% and 1.26% under the confinement of CB[8] (Figure S21). Additionally, the CB[7] was also applied to investigate the macrocyclic confinement effect on guests; although the fluorescence intensity of the two guests was enhanced (Figure S22), no red-shift signal was observed, which may be due to the fact that CB[7] included the guests to restrict the movement of the guests but could not form more conjugated structures. Therefore, the macrocyclic confinement effect of CB[8] can not only effectively induce the guests to generate strong luminescence but also lead to the large red-shift of emission peak of the guests. The nanosupramolecular assembly has a large number of positive charges, which may coassemble with the negatively charged hosts to form the functional NIR luminescent system. Therefore, α-cyclodextrin modified hyaluronic acid (Figure S7) was selected as the secondary assembly unit to investigate the cascade confinement effect for the luminescence properties of nanosupramolecular assemblies. Figure 2c,d show that after the addition of HACD, the fluorescence intensity of the two supramolecular conjugates was enhanced 1.8 and 2.3 times, respectively. Furthermore, by the cascade assembly of HACD, the QY of G1 and G2 were further increased from 0.10% and 1.26% to 0.19% and 1.59%, respectively (Figure S21). The effect of assembly confinement on the fluorescence intensity enhancement of G1/CB[8] is inferior to that of G2/CB[8], which may be due to the weaker binding interaction between G2 and CB[8] is easier to further coassemble with HACD by electrostatic interaction to form more compacted nanostructures with further enhanced fluorescence. The other two kinds of anionic macrocycles-amphiphilic calix[4]arene (SC4A) and sulfobutylether-β-cyclo-

https://doi.org/10.1021/acsnano.3c06697
ACS Nano XXXX, XXX, XXX−XXX

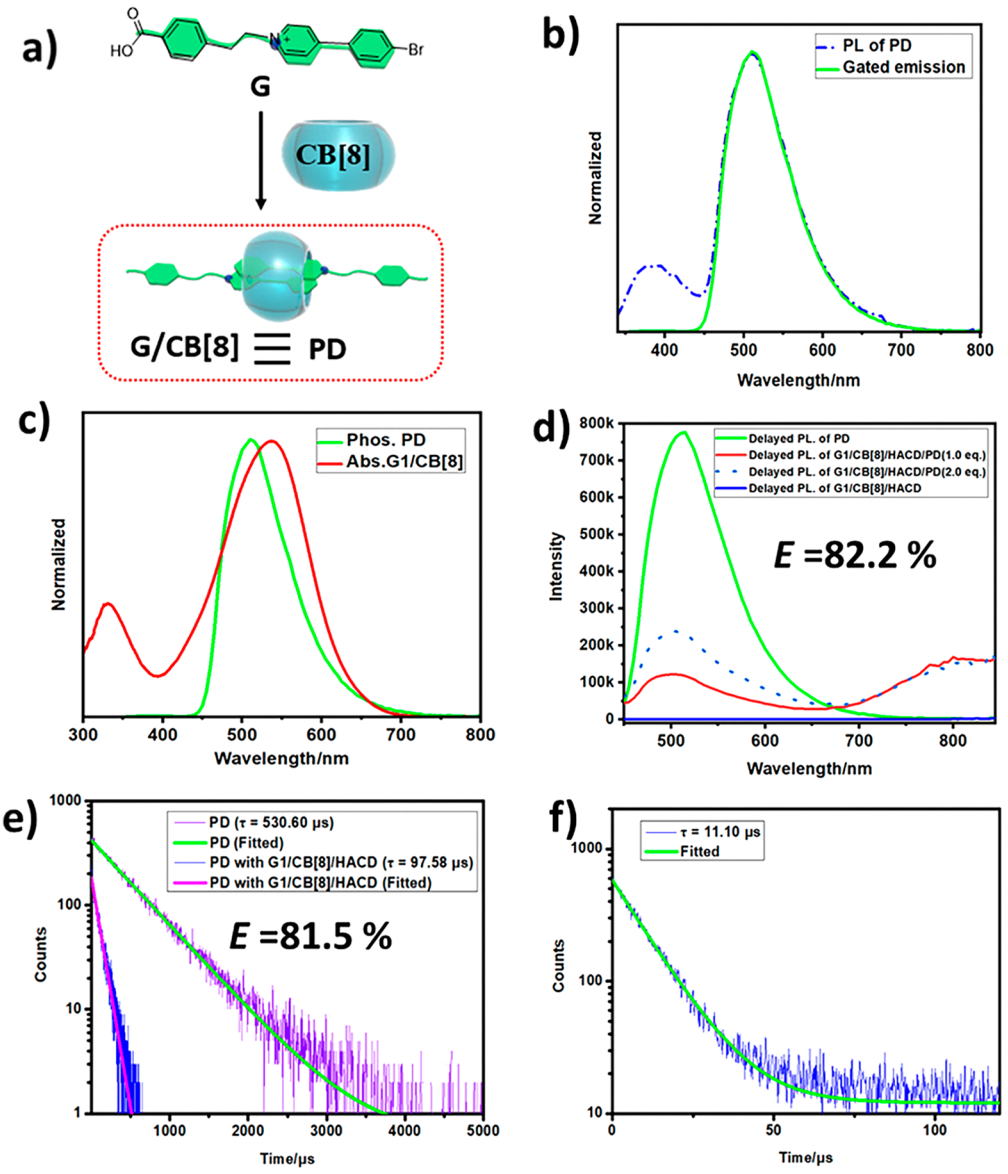

Figure 4. (a) The phosphorescent donor of G/CB[8] (PD). (b) The photoluminescence and phosphorescence spectra (gated emission, delayed 50 μs) of PD (λ_{ex} = 308 nm, [G] = 0.01 mM, [CB[8]] = 0.005 mM). (c) The normalized UV−vis spectrum of G1/CB[8] and phosphorescence spectrum of PD. (d) Delayed photoluminescence spectra of PD, G1/CB[8]/HACD/PD (1.0 and 2.0 equiv) and G1/CB[8]/HACD (λ_{ex} = 308 nm, [G1] = 0.01 mM, [CB[8]] = 0.02 mM, [HACD] = 0.006 mM). (e) Phosphorescence lifetime of PD and G1/CB[8]/HACD/PD (1.0 equiv) at 510 nm (λ_{ex} = 308 nm). (f) Fluorescence lifetime of G1/CB[8]/HACD/PD (1.0 equiv) at 810 nm (λ_{ex} = 308 nm).

dextrin (SBu-CD) were also used to explore the effect of secondary assemble confinement for the luminescence properties of the systems (Figure S23). Figure S24 showed that the fluorescence signal of conjugates was almost unchanged (G1/CB[8]) or enhanced only 1.3 times (G2/CB[8]) in the presence of SC4A. However, with the addition of SBu-CD, the fluorescence intensity of two kinds of supramolecular conjugates decreased to some extent (Figure S25). Therefore, the polysaccharide HACD with carboxyl and hydroxyl groups shows the best assemble confinement enhanced fluorescence effect, which may have occurred because HACD could coassemble with positive nanoassemblies by electrostatic interaction and hydrogen bond to form more favorable confined microenvironment for fluorescence emission. Furthermore, HACD was also added to the solution of guests alone (Figure S26), the fluorescence intensity of guests was also enhanced to some extent, and no red-shift signal was observed, which may be ascribed to the aggregation-induced fluorescence emission enhancement derived from electrostatic interaction between negatively charged HACD and cationic guests. From the above experimental results, it can be seen that the cascade confinement can effectively improve the luminescent properties of the assembly.

Subsequently, transmission electron microscopy (TEM), scanning electron microscopy (SEM), and atomic force microscopy (AFM) were employed to study the topological morphology changes of the supramolecular cascade assembly of two macrocycles. As can be seen from the TEM image (Figure 3a), the G1 was self-assembled to form nanofibers, which gave the same morphology in the SEM test. After the guest was encapsulated by CB[8], the morphology transferred from nanofiber to organic two-dimensional nanosheet as

https://doi.org/10.1021/acsnano.3c06697
ACS Nano XXXX, XXX, XXX−XXX

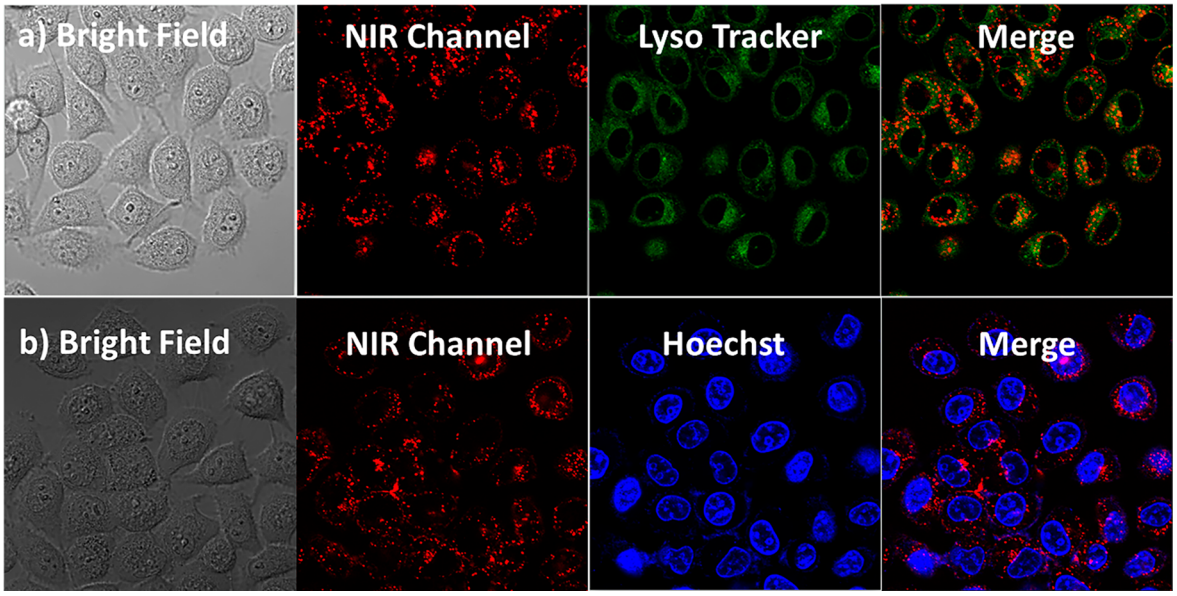

Figure 5. Confocal microscopy images of Hela cells in the presence of G1/CB[8]/HACD/PD and (a) LysoTracker green (lysosome tracker) and (b) Hoechst (the nuclei dye) ([G1] = [PD] = 0.01 mM, [HACD] = 0.006 mM, [CB[8]] = 0.02 mM).

shown in TEM (Figure 3c) and SEM (Figure S27). The performed AFM experiments further confirmed the formation of nanosheets in G1/CB[8]. In particular, the height between the upper and lower layer was measured as 1.78 nm (Figure 3d,e), which was very close to the external diameter (1.75 nm) of CB[8],[29,30] corresponding to the monolayer lamellar assemblies (Figure S28). Although the G2 with short rigid arms was not assembled to form a nanofiber as G1, which was also encapsulated by CB[8] to form the network-like conjugate (Figures S29−S30). Therefore, we can reasonably infer that CB[8] could induce G1 to give "head to tail" like host−guest complexes and noncovalently polymerize into the more extended network-type nanosheet (Figure 3c, inset) and then further layer by layer assembled to form the large thin lamellar assemblies. Assuming the assembly was spherical particles, the sizes of G1/CB[8] and G2/CB[8] calculated from the NMR diffusion coefficients were 3.73 and 3.74 nm, respectively, according to the Stokes−Einstein equation, which was completely different from the sizes measured by DLS experiments. Combining the results of DLS, TEM, SEM, and AFM, we further confirmed that the obtained supramolecular assembly should be the nanosheet. Next, we further explored the influence of HACD assemble confinement on the morphology of the supramolecular conjugates. In sharp contrast with network-like assemblies of G1/CB[8] and G2/CB[8], many irregular nanoparticles were found in the TEM and SEM images of G1/CB[8]/HACD (Figure 3f,g) and G2/CB[8]/HACD (Figure S31), respectively. Therefore, by the cascade confinement, the topological morphology of the assembly was transferred from one-dimensional nanofiber to two-dimensional network-like nanosheet and then to three-dimensional nanoparticles, which also improved the understanding of the relationship between assembly structures and photophysical properties.

From the obtained experimental results, it can be seen that CB[8] confined guests could effectively enhance the fluorescence properties and further coassemble with HACD by multivalent interaction to form nanoparticles, which could not only load energy donors or acceptors but also boost phosphorescent energy transfer, realizing the regulation of NIR luminescence. The highly efficient energy transfer process mainly depended on the phosphorescence behavior of the benzoic acid group modified bromophenylpyridinium salt derivative (G, Figure 4a) under the confinement of CB[8]. Figure 4b demonstrated that the fluorescence signal of G/CB[8] (PD) at 380 nm was not found, and the strong signal still existed (510 nm) in phosphorescence spectroscopy (delayed 50 μs), indicating that the peak at 510 nm should be the long lifetime species. After nitrogen was bubbled in PD solution, the phosphorescence intensity of PD was obviously enhanced (Figure S32a), and the lifetime was increased from 530.60 to 780.92 μs (Figures S32b and S33), indicating the long lifetime signal at 510 nm should be the phosphorescence peak.[31,32] The UV−vis spectroscopy experiments (Figure S34) showed that CB[8] could include G to form a stable 2:1 supramolecular complex (K_s = 1.06 × 10^{11} M^{-2}), and was propitious to the phosphorescence emission of PD. In addition, we also investigated the binding model between the G and CB[8] or α-cyclodextrin (α-CD) by NMR experiments. In Figure S35, the protons of $H_{a,b,c}$ in G/α-CD gave downfield shifts, indicating the benzoic acid group was included by α-CD.[33] Especially, after α-CD was added in the pseudorotaxane (G/CB[8]), the $H_{a,b,c}$ also gave downfield shifts, which should ascribe to the benzoic acid group of the G/CB[8] was included by α-CD, and leading to the positive circular dichroism signal at 225 nm further confirmed that α-CD could bind with PD (Figure S36), then benefiting to the coassemble with the G1/CB[8]/HACD to form a compacted assembly. In Figure 4c, the phosphorescence spectrum of PD well overlapped with the UV−vis spectrum of G1/CB[8], indicating PD may be used as an energy donor.[34] When PD was added into the G1/CB[8]/HACD, a NIR fluorescence signal (810 nm) was observed in delayed photoluminescence spectrum (delayed 50 μs) under the excitation of 308 nm light, but the assembly alone without luminescence peak was observed under the same conditions (Figure 4d). Furthermore, the phosphorescence lifetime of PD (510 nm) decreased from 530.60 to 97.58 μs (Figures 4e and S33), and the lifetime of NIR luminescence peak at 810 nm

https://doi.org/10.1021/acsnano.3c06697
ACS Nano XXXX, XXX, XXX−XXX

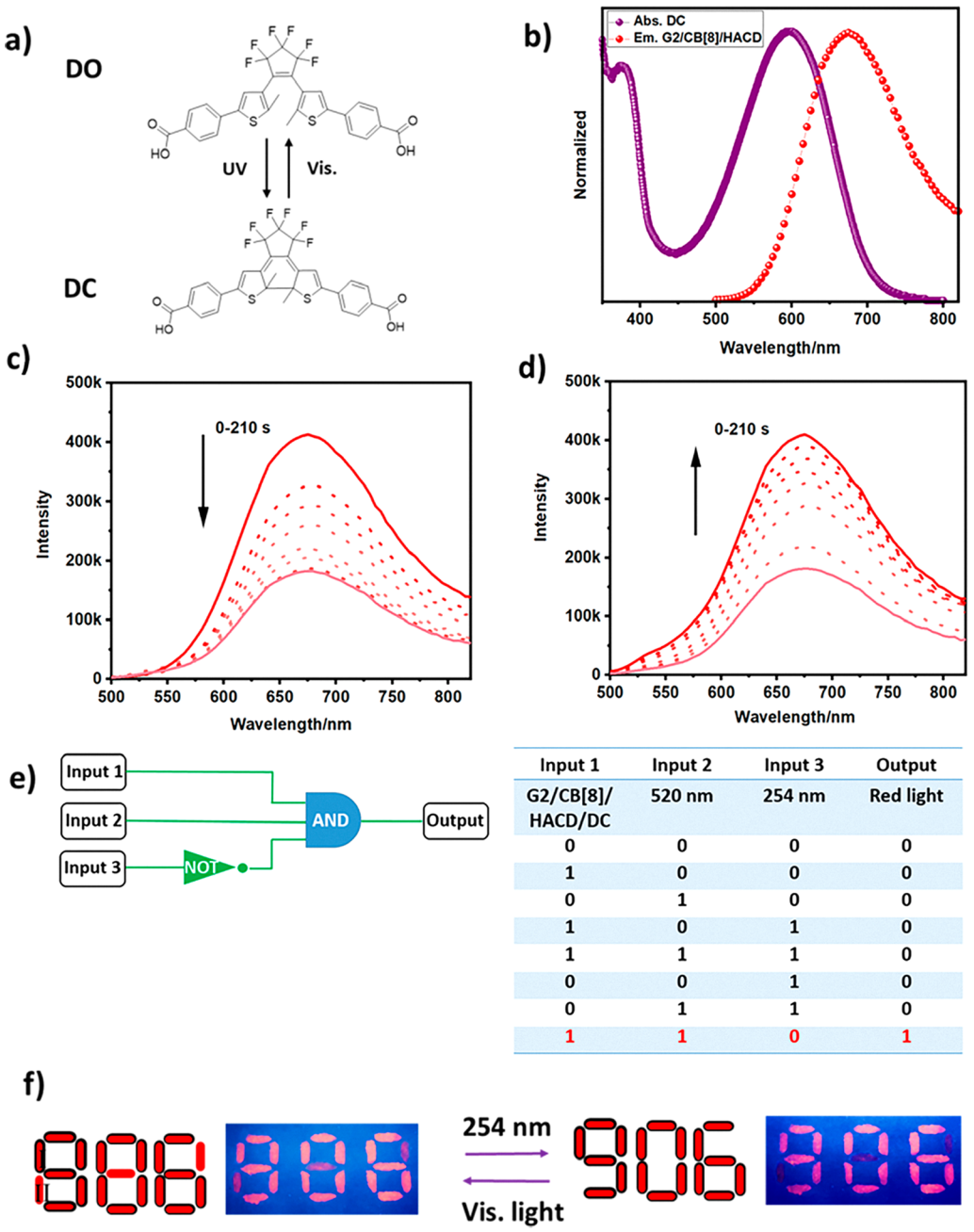

Input 1	Input 2	Input 3	Output
G2/CB[8]/ HACD/DC	520 nm	254 nm	Red light
0	0	0	0
1	0	0	0
0	1	0	0
1	0	1	0
1	1	1	0
0	0	1	0
0	1	1	0
1	1	0	1

Figure 6. (a) Schematic diagram of isomerization of the photoswitch molecule. (b) The normalized absorption spectrum of DC and fluorescence spectrum of G2/CB[8]/HACD. (c) The fluorescence spectra of G2/CB[8]/HACD/DO with 254 nm light irradiation (λ_{ex} = 468 nm, [G2] = [DO] = 0.01 mM, [HACD] = 0.006 mM, and [CB[8]] = 0.02 mM). (d) The fluorescence spectra of G2/CB[8]/ HACD/DC with visible light (>520 nm) irradiation (λ_{ex} = 468 nm, [G2] = [DC] = 0.01 mM, [HACD] = 0.006 mM, [CB[8]] = 0.02 mM). (e) Scheme representation for photoregulated INHIBIT logic gate. (f) The photoresponsive supramolecular fluorescent ink was written in different positions of the numerals (I: G2/CB[8]/HACD; II: G2/CB[8]/HACD/DO).

was measured to be 11.10 μs (Figures 4f and S33), which should ascribe to the energy transfer from long-lived triplet donor to the singlet acceptor then lead to delayed fluorescence emission.[35] According to the change in phosphorescence intensity at 510 nm, the energy transfer efficiency was calculated to be 82.2%, which was very close to the value calculated from the change in donor lifetime (81.5%). After the addition of acceptor, the photoluminescence QY of PD also decreased from 12.46% to 2.67% (Figure S37). In sharp contrast with the above highly efficient energy transfer system, only fairly low energy transfer was observed when HACD was instead used by HA or competitive binder was added (Figure S38). Based on these results, we can reasonably infer that the efficient energy was transferred from phosphorescent PD to noncovalent conjugate in nanoparticles, leading to delayed NIR luminescence at 810 nm with an ultralarge Stokes shifts up to 502 nm.

The NIR luminescent nanoparticles showed the advantages of large Stokes shifts and possessed a targeted cancer moiety (HA), which should be suitable for biological imaging. First, the supramolecular assembly was added in 293T and Hela cells, respectively, and then observed by confocal laser

https://doi.org/10.1021/acsnano.3c06697
ACS Nano XXXX, XXX, XXX−XXX

scanning microscopy. Compared with 293T cells (Figure S39), Hela cells (Figure 5a) gave bright red luminescence, which may be attributed to the fact that the nanoparticle has the hyaluronic acid moiety for targeting cancer cells[36] and then is conducive to the endocytosis of G1/CB[8]/HACD/PD. Furthermore, after incubation with the NIR luminescent nanoparticle, Lyso Tracker green, Hoechst, or Mito Tracker green were added in Hela cells, respectively, to study the ability for targeted organelle imaging. As shown in Figure 5a, the nanoparticle displayed colocalized sites with Lyso Tracker, indicating which could target lysosomes. Figure 5b and S40 showed that this nanoparticle rarely gave colocalization signals with the Hoechst and Mito tracker, indicating that the assembly hardly enters the cell nucleus and mitochondria.

This system takes advantage of the reversible photoisomerization of the diarylethene derivative (Figures 6a and S41), which could act as a photoswitch in the nanoparticle to realize the photoregulation of NIR luminescence. As shown in Figure 6b, the absorption spectrum of the ring-closed DC has a good overlap with the emission peak of G2/CB[8], indicating that the energy transfer process may occur between DC and the luminophore. After the addition of DO, the NIR luminescence of the system gradually decreased with 254 nm light irradiation (Figure 6c), which may be ascribed to the energy transfer from the luminescent noncovalent conjugate to the ring-closed DC (Figure S41).[37] When the system was irradiated with visible light (>520 nm), the fluorescence signal at 670 nm was gradually increased (Figure 6d), which should be attributed to the excited energy of conjugates not being transferred to the ring-opened photoswitch DO. The fluorescence lifetime experiments showed that the lifetime of the assembly at 670 nm was decreased from 3.34 to 1.62 ns after 254 nm light irradiation (Figure S42), and the QY of the system was also decreased from 1.59% to 1.02% (Figure S43), and these results further proved that the energy transferred from noncovalent conjugates to DC. The NIR supramolecular assembly based on cascade confinement showed good photoregulated properties, which may be applied in photoresponsive logic gates, information encryption, and anticounterfeiting materials. The NIR luminescent supramolecular assembly and different wavelength light irradiation were defined as inputs; the red luminescence was defined as outputs (Figure 6e). The fluorescence intensity at 670 nm more than 200 k was defined as "1", and below that was "0". After 254 nm light irradiation, the fluorescence intensity of the supramolecular assembly was no more than 200 k, and the signal could not output; thus, the 254 nm light was set as "NOT" gate. This simple photoresponsive logic gate can output more information and is possibly used as a complex logic gate circuit. Furthermore, we also explored it as photocontrolled fluorescent ink for information encryption. As shown in Figure 6f, the assemblies of G2/CB[8]/HACD and G2/CB[8]/HACD/DO were written in different positions of the numerals, and the signal "888" was found under 450 nm light. After 254 nm irradiation, the real number "906" was observed, which was also concealed after visible light treatment.

CONCLUSION

In conclusion, NIR luminescence and morphology tunable supramolecules were successfully fabricated by the cascade confinement strategy of CB[8] and α-cyclodextrin-grafted hyaluronic acid. Based on strong host−guest interaction, the confinement effect of CB[8] could effectively activate aromatic bridged bis(triphenylamine) derivatives to generate strong NIR luminescence and induce nanofibers of G1 or unaggregated G2 to assemble to form network-like supramolecular conjugates. By the secondary assembly with HACD, the organic two-dimensional nanosheets were transferred to nanoparticles with enhanced NIR emission, which further coassemble with phosphorescent bromophenylpyridine derivative/CB[8] pseudorotaxane or photoswitch diarylethene derivatives to give delayed NIR fluorescence and realize photoregulation of red luminescence, respectively. The tunable nanoassemblies based on cascade confinement were successfully applied in targeted lysosome imaging, photoregulated logic gate, and information encryption, which provide a convenient path for functional NIR luminescent materials.

EXPERIMENTAL SECTION

Materials. The chemicals and solvents were purchased from HEOWNS. Silica gel (200−300 mush) and thin layer chromatography (TLC, GF254) were applied to chromatographic purification and monitoring of the reaction, respectively. The 293T cells and Hela cells were purchased from the Cell Resource Center, China Academy of Medical Science Beijing, China.

Measurements. The NMR data were collected from the Bruker Avance spectrometers; chemical shifts (δ) were labeled as parts per million, and the internal standard compound was TMS. The fluorescence and quantum yield experiments were studied on Edinburgh Instrument FS5. The JEOL JSM-7500F instrument with an accelerating voltage of 30 keV was applied to collect the SEM pictures. The Philips Tecnai G2 20 S-TWIN microscope (HRTEM) was used to study the TEM experiments. AFM images were carried out with Bruker Dimension Ion AMF. Olympus FV1000 Laser scanning confocal microscope and Leika S8 microscope were applied to observe the cell images. Hydrodynamic sizes were collected from a laser light scattering spectrometer (BI-200SM).

The Synthesis of Compound 2 (Scheme S1). Compound 1 (1.00 g, 1.37 mmol) and 4-vinylpyridine (1.16 g, 10.99 mmol) were added to the anhydrous DMF, and then the palladium(II) acetate (123 mg, 0.55 mmol), tri-*o*-tolylphosphine (167 mg, 0.55 mmol), and TEA (5 mL) were added in the above solution under N_2, which was refluxed for 48 h, then cooled to room temperature, added to the water, and extracted by dichloromethane. The obtained dichloromethane solution was further treated with water and sodium chloride solution, then evaporated under vacuum, and purified by column chromatography to give 2 (0.32 g, yield: 24.6%). ^{1}H NMR (400 MHz, $CDCl_3$) δ 8.56 (s, 8H), 7.47 (d, J = 8.5 Hz, 8H), 7.35 (d, J = 5.0 Hz, 8H), 7.27 (t, J = 16.3 Hz, 4H), 7.15 (d, J = 8.5 Hz, 8H), 7.09 (s, 4H), 6.93 (d, J = 16.3 Hz, 4H).

The Synthesis of G1. Compound 2 (200 mg, 0.24 mmol) was dissolved in DMF, and then CH_3I (2 mL) was injected and heated at 50 °C for 12 h under N_2, which was further poured in ethyl acetate to obtain the precipitate, which was further dissolved in water and saturated KPF_6 solution was added to give hexafluorophosphate salt of G1 as precipitate. Then, Bu_4NBr was added to the CH_3CN solution of hexafluorophosphate salt of G1 to give a red precipitate, filtrated, and then dried to give G1 (213 mg, yield 72.9%). ^{1}H NMR (400 MHz, $(CD_3)_2SO$): δ 8.83 (d, J = 6.5 Hz, 8H), 8.19 (d, J = 6.2 Hz, 8H), 8.01 (d, J = 16.1 Hz, 4H), 7.74 (d, J = 8.3 Hz, 8H), 7.41 (d, J = 16.1 Hz, 4H), 7.19 (d, J = 6.4 Hz, 12H), 4.24 (s, 12H). ^{13}C NMR (100 MHz, $(CD_3)_2SO$): δ 153.13, 148.69, 145.43, 142.76, 140.61, 130.46, 130.31, 127.44, 123.79, 123.64, 122.11, 47.26. HR-MS (ESI): m/z for $C_{62}H_{56}N_6Br_4$ calcd. $[M\text{-}4Br]^{4+}$ = 211.1136, found: 221.1138.

The Synthesis of G. 4-(4-Bromophenyl) pyridine (0.17 g, 0.73 mmol) and 4-(2-bromoethyl) benzoic acid (0.20 g, 0.87 mmol) were dissolved in CH_3CN and heated at 80 °C in a sealed tube for 12 h. After cooling to room temperature, diethyl ether was added to the above mixture to give precipitate, filtrated, and then dried to give G (0.20 g, yield: 59.5%). ^{1}H NMR (400 MHz, $(CD_3)_2SO$) δ: 9.07 (d, J

https://doi.org/10.1021/acsnano.3c06697
ACS Nano XXXX, XXX, XXX−XXX

= 6.9 Hz, 2H), 8.54 (d, J = 6.9 Hz, 2H), 8.04 (d, J = 8.7 Hz, 2H), 7.88−7.85 (m, 4H), 7.39 (d, J = 8.2 Hz, 2H), 4.88 (t, J = 7.4 Hz, 2H). ^{13}C NMR (100 MHz, $(CD_3)_2SO$) δ: 167.56, 154.08, 145.42, 141.95, 133.11, 133.06, 130.66, 130.09, 130.03, 129.72, 126.80, 124.79, 60.66, 36.75. HR-MS (ESI): m/z for $C_{20}H_{17}NBr_2O_2$ calcd. $[M\text{-}Br]^+$ = 382.0437, found: 382.04366.

Cell Imaging Experiments. Hela cells were precultured for 24 h, and then G1/CB[8]/HACD/PD was added and further incubated for 12 h. After that, the Hoechst, LysoTracker green, or MitoTracker green were added in cells, respectively, washed with PBS three times, and then further investigated by confocal laser scanning microscopy.

ASSOCIATED CONTENT

Supporting Information

The Supporting Information is available free of charge at https://pubs.acs.org/doi/10.1021/acsnano.3c06697.

Synthesis route (Scheme S1), NMR and MS data (Figures S1−S10), Job plots (Figure S11), UV−vis spectra and binding constants (Figures S12−S13), ^{1}H NMR titration spectra (Figures S14−S15), 2D NOESY and DOSY spectra (Figures S16−S19), DLS data (Figures S20), quantum yields (Figures S21), fluorescence spectra (Figures S22, S24−S26), anionic macrocyclic hosts (Figures S23), SEM, TEM, and AFM images (Figures S27−S31), photoluminescence spectra and lifetime (Figures S32−S33), UV−visible spectra, Job plot, and binding constants (Figures S34), ^{1}H NMR spectra (Figures S35), circular dichroism spectra (Figures S36), quantum yields (Figures S37), photoluminescence spectra (Figures S38), confocal microscopy images (Figures S39−40), UV−visible spectra (Figure 41), fluorescence lifetime and quantum yields (Figures S42−S43) (PDF)

AUTHOR INFORMATION

Corresponding Author

Yu Liu − *College of Chemistry, State Key Laboratory of Elemento-Organic Chemistry, Nankai University, Tianjin 300071, China*; orcid.org/0000-0001-8723-1896; Email: yuliu@nankai.edu.cn

Authors

Jie Yu − *College of Chemistry, State Key Laboratory of Elemento-Organic Chemistry, Nankai University, Tianjin 300071, China*

Jie Niu − *College of Chemistry, State Key Laboratory of Elemento-Organic Chemistry, Nankai University, Tianjin 300071, China*

Jinlong Yue − *College of Chemistry, State Key Laboratory of Elemento-Organic Chemistry, Nankai University, Tianjin 300071, China*

Li-Hua Wang − *College of Chemistry, State Key Laboratory of Elemento-Organic Chemistry, Nankai University, Tianjin 300071, China*

Complete contact information is available at: https://pubs.acs.org/10.1021/acsnano.3c06697

Author Contributions

J.Yu, J.N., J.Yue, and L.-H.W. synthesized the compounds and performed experiments. J.Yu collected data, summarized, and wrote the work. The work was supervised by Y.L.

Funding

National Natural Science Foundation of China (22201142 and 22131008).

Notes

The authors declare no competing financial interest.

ACKNOWLEDGMENTS

We thank the National Natural Science Foundation of China (22201142 and 22131008) for financial support.

REFERENCES

(1) Zhao, Z.; Zhang, H.; Lam, J. W. Y.; Tang, B. Z. Aggregation-Induced Emission: New vistas at the aggregate level. *Angew. Chem., Int. Ed.* **2020**, *59*, 9888−9907.

(2) Yanai, N.; Kimizuka, N. Recent emergence of photon upconversion based on triplet energy migration in molecular assemblies. *Chem. Commun.* **2016**, *52*, 5354−5370.

(3) Shigemitsu, H.; Tani, Y.; Tamemoto, T.; Mori, T.; Li, X.; Osakada, Y.; Fujitsuka, M.; Kida, T. Aggregation-induced photocatalytic activity and efficient photocatalytic hydrogen evolution of amphiphilic rhodamines in water. *Chem. Sci.* **2020**, *11*, 11843−11848.

(4) Shigemitsu, H.; Tamemoto, T.; Ohkubo, K.; Mori, T.; Osakada, Y.; Fujitsuka, M.; Kida, T. A cyanine dye based supramolecular photosensitizer enabling visible-light-driven organic reaction in water. *Chem. Commun.* **2021**, *57*, 11217−11220.

(5) Shigemitsu, H.; Ohkubo, K.; Sato, K.; Bunno, A.; Mori, T.; Osakada, Y.; Fujitsuka, M.; Kida, T. Fluorescein-based type I supramolecular photosensitizer via induction of charge separation by self-assembly. *JACS Au* **2022**, *2*, 1472−1478.

(6) Martins, J. N.; Raimundo, B.; Rioboo, A.; Folgar-Cameán, Y.; Montenegro, J.; Basílio, N. Photoswitchable calixarene activators for controlled peptide transport across lipid membranes. *J. Am. Chem. Soc.* **2023**, *145*, 13126−13133.

(7) Gu, M.-J.; Han, X.-N.; Guo, W.-C.; Han, Y.; Chen, C.-F. Naphth[4]arene: synthesis, conformations, and application in color-tunable supramolecular crystalline assemblies. *Angew. Chem., Int. Ed.* **2023**, No. e202305214.

(8) Xie, F.; Mao, H.; Lin, C.; Feng, Y.; Stoddart, J. F.; Young, R. M.; Wasielewski, M. R. Quantum sensing of electric fields using spin-correlated radical ion pairs. *J. Am. Chem. Soc.* **2023**, *145*, 14922−14931.

(9) Liu, C.; Morimoto, N.; Jiang, L.; Kawahara, S.; Noritomi, T.; Yokoyama, H.; Mayumi, K.; Ito, K. Tough hydrogels with rapid self-reinforcement. *Science* **2021**, *372*, 1078−1081.

(10) Li, T.-R.; Huck, F.; Piccini, G. M.; Tiefenbacher, K. Mimicry of the proton wire mechanism of enzymes inside a supramolecular capsule enables β-selectiven o-glycosylations. *Nat. Chem.* **2022**, *14*, 985−994.

(11) Jiang, Z.; Dong, R.; Evans, A. M.; Biere, N.; Ebrahim, M. A.; Li, S.; Anselmetti, D.; Dichtel, W. R.; Livingston, A. G. Aligned macrocycle pores in ultrathin films for accurate molecular sieving. *Nature* **2022**, *609*, 58−64.

(12) Mukhopadhyay, R. D.; Kim, K. Cucurbituril curiosities. *Nat. Chem.* **2023**, *15*, 438.

(13) Kim, D.; Aktalay, A.; Jensen, N.; Uno, K.; Bossi, M. L.; Belov, V. N.; Hell, S. W. Supramolecular complex of photochromic diarylethene and cucurbit[7]uril: fluorescent photoswitching system for biolabeling and imaging. *J. Am. Chem. Soc.* **2022**, *144*, 14235−14247.

(14) Wu, G.; Bae, Y. J.; Olesińska, M.; Antón-García, D.; Szabó, I.; Rosta, E.; Wasielewski, M.; Scherman, R. O. A. Controlling the structure and photophysics of fluorophore dimers using multiple cucurbit[8]uril clampings. *Chem. Sci.* **2020**, *11*, 812−825.

(15) Garain, S.; Garain, B. C.; Eswaramoorthy, M.; Pati, S. K.; George, S. J. Light-harvesting supramolecular phosphors: highly efficient room temperature phosphorescence in solution and hydrogels. *Angew. Chem., Int. Ed.* **2021**, *60*, 19720−19724.

(16) Chen, X.; Bisoyi, H. K.; Chen, X.-F.; Chen, X.-M.; Zhang, S.; Tang, Y.; Zhu, G.; Yang, H.; Li, Q. Hierarchical self-assembly of an excitation wavelength-dependent emissive fluorophore and cucurbiturils for secondary encryption. *Matter* **2022**, *5*, 3883−3900.
(17) Yu, H.-J.; Zhou, Q.; Dai, X.; Shen, F.-F.; Zhang, Y.-M.; Xu, X.; Liu, Y. Photooxidation-driven purely organic room-temperature phosphorescent lysosome-targeted imaging. *J. Am. Chem. Soc.* **2021**, *143*, 13887−13894.
(18) Votava, M.; Ravoo, B. J. Principles and applications of cyclodextrin liquid crystals. *Chem. Soc. Rev.* **2021**, *50*, 10009−10024.
(19) Shigemitsu, H.; Kawakami, K.; Nagata, Y.; Kajiwara, R.; Yamada, S.; Mori, T.; Kida, T. Cyclodextrins with multiple pyrenyl groups: an approach to organic molecules exhibiting bright excimer circularly polarized luminescence. *Angew. Chem., Int. Ed.* **2022**, *61*, No. e202114700.
(20) Li, D.; Liu, Z.; Fang, M.; Yang, J.; Tang, B. Z.; Li, Z. Ultralong room-temperature phosphorescence with second-level lifetime in water based on cyclodextrin supramolecular assembly. *ACS Nano* **2023**, *17*, 12895−12902.
(21) Ma, X.-K.; Cheng, Q.; Zhou, X.; Liu, Y. Macrocycle γ-cyclodextrin confined polymeric chromophore ultralong phosphorescence energy transfer. *JACS Au* **2023**, *3*, 2036−2043.
(22) Tian, M.; Wang, Z.; Yuan, X.; Zhang, H.; Liu, Z.; Liu, Y. Configurationally confined multilevel supramolecular assemblies for modulating multicolor luminescence. *Adv. Funct. Mater.* **2023**, *33*, 2300779.
(23) Chen, X.-M.; Chen, Y.; Yu, Q.-L.; Gu, B.-H.; Liu, Y. Supramolecular assemblies with near-infrared emission mediated in two stages by cucurbituril and amphiphilic calixarene for lysosome-targeted cell imaging. *Angew. Chem., Int. Ed.* **2018**, *57*, 12519−12523.
(24) Sar, D.; Ostadhossein, F.; Moitra, P.; Alafeef, M.; Pan, D. Small molecule NIR-II dyes for switchable photoluminescence via host-guest complexation and supramolecular assembly with carbon dots. *Adv. Sci.* **2022**, *9*, 2202414.
(25) Schoder, S.; Schröder, H. V.; Cera, L.; Puttreddy, R.; Güttler, A.; Resch-Genger, U.; Rissanen, K.; Schalley, C. A. Strong emission enhancement in pH-responsive 2:2 cucurbit[8]uril complexes. *Chem.—Eur. J.* **2019**, *25*, 3257−3261.
(26) Assaf, K. I.; Alnajjar, M. A.; Nau, W. M. Supramolecular assemblies through host-guest complexation between cucurbiturils and an amphiphilic guest molecule. *Chem. Commun.* **2018**, *54*, 1734−1737.
(27) Li, Y.; Dong, Y.; Miao, X.; Ren, Y.; Zhang, B.; Wang, P.; Yu, Y.; Li, B.; Isaacs, L.; Cao, L. Shape-controllable and fluorescent supramolecular organic frameworks through aqueous host-guest complexation. *Angew. Chem., Int. Ed.* **2018**, *57*, 729−733.
(28) Zhang, K. D.; Tian, J.; Hanifi, D.; Zhang, Y. B.; Sue, A. C.; Zhou, T. Y.; Zhang, L.; Zhao, X.; Liu, Y.; Li, Z. T. Toward a single-layer two-dimensional honeycomb supramolecular organic framework in water. *J. Am. Chem. Soc.* **2013**, *135*, 17913−17918.
(29) Yu, J.; Wang, H.; Dai, X.; Chen, Y.; Liu, Y. Multivalent supramolecular assembly based on a triphenylamine derivative for near-infrared lysosome targeted imaging. *ACS Appl. Mater. Interfaces* **2022**, *14*, 4417−4422.
(30) Kim, K.; Selvapalam, N.; Ko, Y. H.; Park, K. M.; Kim, D.; Kim, J. Functionalized cucurbiturils and their applications. *Chem. Soc. Rev.* **2007**, *36*, 267−279.
(31) Garain, S.; Sarkar, S.; Garain, B. C.; Pati, S. K.; George, S. J. Chiral arylene diimide phosphors: circularly polarized ambient phosphorescence from bischromophoric pyromellitic diimides. *Angew. Chem., Int. Ed.* **2022**, *61*, No. e202115773.
(32) Yu, J.; Wang, H.; Liu, Y. Double-network confined supramolecular phosphorescence light-harvesting boosting photocatalysis. *Adv. Opt. Mater.* **2022**, *10*, 2201761.
(33) Morin-Crini, N.; Fourmentin, S.; Fenyvesi, E.; Lichtfouse, E.; Torri, G.; Fourmentin, M.; Crini, G. 130 years of cyclodextrin discovery for health, food, agriculture, and the industry: a review. *Environ. Chem. Lett.* **2021**, *19*, 2581−2617.
(34) Hao, M.; Sun, G.; Zuo, M.; Xu, Z.; Chen, Y.; Hu, X.-Y.; Wang, L. A supramolecular artificial light-harvesting system with two-step sequential energy transfer for photochemical catalysis. *Angew. Chem., Int. Ed.* **2020**, *59*, 10095−10100.
(35) Li, D.; Yang, J.; Fang, M.; Tang, B. Z.; Li, Z. Stimulus-responsive room temperature phosphorescence materials with full-color tenability from pure organic amorphous polymers. *Sci. Adv.* **2022**, *8*, No. eabl8392.
(36) Choi, K. Y.; Han, H. S.; Lee, E. S.; Shin, J. M.; Almquist, B. D.; Lee, D. S.; Park, J. H. Hyaluronic acid-based activatable nanomaterials for stimuli-responsive imaging and therapeutics: beyond cd44-mediated drug delivery. *Adv. Mater.* **2019**, *31*, 1803549.
(37) Ma, L.; Xu, Q.; Sun, S.; Ding, B.; Huang, Z.; Ma, X.; Tian, H. A universal strategy for tunable persistent luminescent materials via radiative energy transfer. *Angew. Chem., Int. Ed.* **2022**, *61*, No. e202115748.

https://doi.org/10.1021/acsnano.3c06697
ACS Nano XXXX, XXX, XXX−XXX